

$^{28}\text{SiO } \nu = 1$ and $\nu = 2$, $J = 1-0$ maser variability in evolved stars. Eleven years of short spaced monitoring[★]

J. R. Pardo^{1,2}, J. Alcolea², V. Bujarrabal², F. Colomer², A. del Romero^{3,2}, and P. de Vicente²

¹ Departamento de Astrofísica Molecular e Infrarroja, Instituto de Estructura de la Materia, CSIC, Serrano 121, 28006 Madrid, Spain
e-mail: pardo@damir.iem.csic.es

² Observatorio Astronómico Nacional, Apartado 1143, 28800 Alcalá de Henares, Spain
e-mail: [j.alcolea;v.bujarrabal;f.colomer;p.devicente]@oan.es

³ Departamento de Física, Universidad de Alcalá de Henares, Campus Universitario, 28871 Alcalá de Henares, Spain
e-mail: armando.delromero@uah.es

Received 20 February 2004 / Accepted 7 May 2004

Abstract. This paper presents and discusses the final data set of a long-term and short-spaced monitoring of 21 SiO maser sources, mostly evolved stars, carried out in two SiO maser lines at 43 GHz with the Observatorio Astronómico Nacional 13.7 m telescope at the Centro Astronómico de Yebes (Guadalajara, Spain). In most objects, more than 80 spectra per transition over a period of 11 years have been recorded. The new data presented here, previously unpublished, represent nearly 50% of the total SiO data collected in the project. In addition, the availability of optical light curves from the AAVSO for most of the objects during the whole period of the SiO monitoring, ground-based near-IR data for four sources overlapping with 3 to 5 observed SiO periods, and DIRBE near-IR data covering a significant portion of an SiO period in 10 sources, make this data set a unique reference for comparing optical, NIR and SiO variability in order to elucidate the physical mechanisms that pump SiO masers in evolved stars. The basis for the conclusions obtained in this work comes from a numerical time series analysis of the suitable SiO, optical and NIR light curves in regular variables to obtain precise values of the periods and phase lags between the different curves. This analysis shows evidence that in regular variable evolved stars the three types of emission have the same period and that the SiO maxima happen in phase with NIR maxima and with a phase lag typically between 0.05 and 0.20 with respect to optical maxima. We conclude that in these objects the observational evidence presented in this work favors the radiative pumping of SiO masers against the collisional pumping.

Key words. stars: late type – masers – stars: AGB and post-AGB – radio lines: stars

1. Introduction

The rotational transitions within vibrationally excited states of ^{28}SiO (SiO hereafter) show intense maser emission in objects such as AGB stars, mostly O-rich Mira-type variables, as well as in a few star-forming regions. More than 1000 emitters have been reported since the discovery of this emission by Snyder & Buhl (1974), including extragalactic sources (van Loon et al. 1996). In oxygen-rich Mira-type variables OH, H₂O and SiO maser emissions are common, the latter arising closest to the star within the circumstellar shell at a few stellar radii (Diamond et al. 1994) and showing strong variations (e.g. Hjalmarsen & Olofsson 1979; Lane 1982; Nyman & Olofsson 1986). The SiO masers involve rotational transitions inside excited vibration states, high above the ground state. The energy levels involved can maintain the necessary populations to produce a maser only relatively close to the star. The environment

is thus complex and this complexity is expected to show up in the behavior of the SiO masers.

Short-spaced, long-term monitoring of SiO maser emission is a necessary tool to characterize the variability of SiO maser emission, one of its most remarkable properties revealed since the earliest studies (e.g. Hjalmarsen & Olofsson 1979; Lane 1982; Nyman & Olofsson 1986), with the ultimate goal of understanding the pumping mechanisms involved. These mechanisms are termed collisional or radiative according to the nature of the process that dominates the molecular excitation up to the vibrationally excited levels. Both types of pumping can in principle produce the required inversion resulting in SiO masers under the appropriate conditions. They can work simultaneously or, in specific circumstances, only one may produce the inversion. The nature of the pump in any particular source is determined by the relative strengths of the two mechanisms.

[★] Figures 1–4 and 11–21 are only available in electronic form at <http://www.edpsciences.org>

– **Radiative pumping models** assume that the energy emitted by the masers comes from the stellar continuum

at $\lambda \approx 8 \mu\text{m}$, absorbed by circumstellar SiO molecules through $\Delta v = 1$ vibrational transitions (see for example Bujarrabal 1994a or Rausch et al. 1996 for an alternative model). Radiative pump models relate the number of photons in the maser transition and in the pump bandwidth. This dependence on observable quantities make these models more easily confrontable with observations. In fact, the masers whose detailed modeling has been most successful are the OH masers in late-type stars because they are pumped by infrared radiation resulting from the reemission of the stellar radiation by the dust particles located in the stellar wind.

- **Collisional pumping models** relate SiO maser maxima with the arrival in the emitting region of a shock front generated by the stellar pulsation. The stellar oscillation is driven by a sinusoidally varying force situated below the photosphere of the star (Humphreys et al. 2002). Relating the model phase to the stellar optical phase has the difficulty that the first one is in principle not derivable from observations.

The earliest SiO maser variability monitorings confirmed that SiO maser variability in O-rich Mira-type stars has approximately the same period as their optical light-curves, which are available for several decades for many objects (<http://www.aavso.org/vstar/>), and indicated the possible presence of an SiO-optical phase lag of ~ 0.1 – 0.2 periods (see e.g. Hjalmarsen & Olofsson 1979; Lane 1982; Nyman & Olofsson 1986). Independently, some works indicated similar phase lags between near-IR and optical light curves in Mira-type variable stars (Le Bertre 1993, hereafter LeB93; and Smith et al. 2002, 2003, hereafter SMI03). Recent SiO monitoring efforts have focused on the spatial distribution of the masing cells (Diamond & Kemball 2003), on their polarization characteristics (Glenn et al. 2003; Cotton et al. 2004), and on the high velocity line wing activity (Herpin et al. 1998).

The short time-spaced monitoring presented in this paper started in July 1984 and ended in April 1995. The initial aim of the project was to acquire a single well calibrated spectrum of two different SiO lines: $v = 1$ and $v = 2$ $J = 1-0$ (7 mm wavelength) in a sample of objects (see Table 1), mostly evolved stars, every 3–4 weeks using the Observatorio Astronómico Nacional 13.7 m telescope at the Centro Astronómico de Yebes (Guadalajara, Spain). This overall goal was achieved, although we have to report some program changes and shutdown periods during the 11-year span of the project (see Sect. 2). Initially, the monitoring included 14 sources. This number increased to 21 in 1989. The sample was made up of Mira-type variables, semiregular AGB stars, red supergiants and one star-forming region (Orion IRc2). In the observations, particular attention was paid to ensuring a proper relative calibration during the whole 11-year period.

We have published so far all the data acquired prior to May 1990 (see Martínez et al. 1988, hereafter MAR88; and Alcolea et al. 1999, hereafter ALC99). These published data already confirmed the earlier results by Hjalmarsen & Olofsson (1979), Lane (1982), and Nyman & Olofsson (1986) but making a stronger case. For instance, ALC99 presented a total of

about 1800 spectra, to be compared with at most ~ 300 spectra presented in the previous studies. In a few objects, for which near-IR variability had been at least partially simultaneously monitored (LeB93), ALC99 directly found a tight relation between the NIR and SiO maxima.

The SiO curves in several objects presented in ALC99 were found to have a poor reproducibility. Often, epochs with strong fluxes and flux variations alternated with others in which even the maxima were poorly detected. In other cases, however, the line profiles kept basically the same features during much longer times than the stellar period. In others they showed strong and often relatively fast variations. We were also able to conclude that the supergiant VX Sgr, and specially the semiregular star GY Aql, both with high and periodic optical variability, have SiO variations with a phase lag comparable to that found in Mira-type variables. However, in VY CMa, μ Cep and RT Vir, the published data did not cover a long enough period of time to allow any conclusion. Also in some Mira-type variables, in particular in two interesting objects, the S-type star χ Cyg and the long-period OH/IR star OH 26.5+0.6, the published monitoring was certainly too short to allow any conclusions on the properties of their SiO light curves.

In this paper we present the complete Yebes monitoring results, including more than 3500 spectra recorded over a 11 year period (1984–1995). We note that spectra obtained after January 1989 have a much better signal-to-noise ratio than those recorded prior to that date, due to the implementation of a low-temperature cooled receiver at the telescope (Sect. 2). This makes the 1990–1995 period of the monitoring, first published here, far more significant than the previously published data, and this is even more dramatic for objects included in the monitoring in 1989.

In Sect. 2 we summarize the observing method (fully described in MAR88 and ALC99). Section 3 is devoted to describe the time-series analysis of the SiO and complementary data sets used for later discussions. The discussions in Sect. 4 focus on groups of objects, especially on regular variable stars. Finally, the conclusions are given in Sect. 5.

2. Observing method, relative calibration and final data set

The 43 GHz (7 mm) maser emission in the vibrationally excited $v = 1$ and $v = 2$ states of SiO has been monitored with the Observatorio Astronómico Nacional 13.7 m telescope at the Centro Astronómico de Yebes (Guadalajara, Spain, 980 m above sea level) for a maximum time span of almost 11 years (14 objects in the $v = 1$, $J = 1-0$ SiO transition monitored between July 1984 and April 1995). The goal was to record between 10 and 15 spectra per pulsation cycle in Mira-type variables, the dominant group in the sample. There was only one major shutdown period in this project: ~ 3 months in 1988 to replace the receiver (see below). The lower system temperature of the new receiver reduced integration times and made it possible to add new sources to the project to reach a total of 21 (see the object sample in Table 1). The detected polarization as well as antenna efficiency with elevation also suffered changes during the project, but were properly measured,

Table 1. The sample of objects of the SiO monitoring presented in this paper and the time sampling achieved for each of them.

Name (type ¹)	coordinates		$\nu = 1;2$		Figures
	RA	Dec	Av. sampling (days)	Num. spectra	
	(1950)	(1950)			
ρ Cet (M)	02 16 49.0	-03 12 13	29;41	125;86	5, 8
IK Tau (M)	03 50 43.6	+11 15 32	30;39	116;87	5, 10
TX Cam (M)	04 56 43.0	+56 06 48	31;45	121;66	??*
R Cnc (M)	08 13 48.6	+11 52 52	38;46	60;49	??*
X Hya (M)	09 33 06.7	-14 28 05	39;45	61;48	
R LMi (M)	09 42 35.0	+34 44 34	31;40	119;86	??*
R Leo (M)	09 44 52.2	+11 39 40	32;39	118;87	5, ??*
W Hya (M)	13 46 12.0	-28 07 06	30;38	121;87	??*
U Her (M)	16 23 35.0	+19 00 18	32;38	117;87	??*
R Aql (M)	19 03 57.7	+08 09 08	38;37	61;49	??*
χ Cyg (M)	19 48 38.4	+32 47 10	36;50	62;45	
R Aqr (M)	23 41 14.0	-15 33 42	32;39	118;85	5, ??*
R Cas (M)	23 55 52.0	+51 06 37	30;41	123;67	5, ??*
IRC+10011 (OH/IR)	01 03 48.0	+12 19 51	33;49	79;59	??*
OH 26.5+0.6 (OH/IR)	18 34 52.5	-05 26 37	40;47	58;48	??*
RT Vir (SR)	13 00 05.8	+05 27 14	31;41	108;64	
GY Aql (SR ²)	19 47 25.0	-07 44 30	31;42	119;86	5, 9
VY CMa (SG)	07 20 55.0	-25 40 12	32;42	115;83	2*
VX Sgr (SG)	18 05 03.0	-22 13 55	31;41	117;63	3*
μ Cep (SG)	21 41 58.5	+58 33 01	34;42	78;61	4*
Orion IRc2 (SFR)	05 32 47.0	-05 24 23	30;41	122;92	1*

Notes.- ¹ SG: Supergiant, SR: Semiregular, Mi: Mira-type, OH/IR: OH/IR star, SFR: Star Forming Region.

² The data presented here suggest a Mira-type behavior.

* These figures available only online.

modeled and taken into account in the calibration procedure. All technical details involved in the observations were described in detail in ALC99. We will only quickly summarize them here:

- **Receiver characteristics:** Schottky diode balanced mixer and FET amplifier. First, at room temperature (SSB $T_{a,sys}^*$, defined in ALC99, of about 900 to 600 K) before December 1988. Afterward, the new Schottky diode was cooled down to 20 K yielding SSB $T_{a,sys}^*$ of 260 K. Simultaneously with the receiver change, a $\lambda/4$ plate was added to ensure reception of left-hand circular polarization in order to avoid effects due to the strong linear polarization of SiO masers. Note that in this paper we present 5 years of data obtained with the last, much improved, configuration. The remaining 1.5 years of data obtained in this configuration were already presented in ALC99. For more details on measurements of SiO maser polarization, please see Barvainis et al. (1987), Glenn et al. (2003), and Cotton et al. (2004).
- **Spectrometer:** 256 channels filter bank (50 kHz per channel), 0.35 km s^{-1} resolution degraded to 0.7 km s^{-1} for the analysis.
- **Observing mode:** frequency switching by 6.4 MHz. This reduces the total filter bank bandwidth to 44 km^{-1} . Position switching for only three objects (VY CMa, VX Sgr and Orion IRc2) with an off position 10 arcmin away in azimuth (the beam size is ~ 2 arcmin).
- **Calibration of the spectra:** procedure explained in Barcia et al. (1985).

- **Conversion factor from antenna temperature to flux in Jy** obtained from observations of the planets as calibrators.

The relative calibration of data recorded over several years is a key issue in this project. Different actions were undertaken to ensure the best possible relative calibration. ALC99 described them all in detail.

- **Pointing.** Each source was observed in five different positions separated by 30 arcsec forming a cross on the sky. Assuming a Gaussian beam, pointing errors were calculated and the proper correction was applied to the spectrum finally stored in the database.
- **Polarization.** Each source was always observed at similar hour angle to avoid artificial variability due to changes in the telescope efficiency with elevation or by linear polarization (prior to December 1988) in the signal and changing parallactic angles (see a detailed discussion in Sect. 3.3 of ALC99).
- **Sky.** The observations were carried out only in clear sky conditions in order to reduce the impact of unstable atmospheric conditions on the calibration.
- **Systematics.** The monitoring of a continuum source (W51) yielded no noticeable systematic or seasonal changes, within data noise, and therefore no corrections were introduced to the SiO data based on these results.

The final data set of the project, presented in this paper, consists of a total of 2118 spectra in $\nu = 1$ and 1485 in $\nu = 2$.

Table 2. Time series analysis for those objects in our sample where SiO periods can be established from our data. The SiO variability of GY Aql, an object considered as a semiregular star at the beginning of the survey, shows all the characteristics found in a typical Mira-type star. All other objects in our sample were not considered in this analysis because no periodicity could be found in the available data.

Name	V1 Max./area			V2 Max./area			Optical or NIR			Period GCVS
	P	W	D	P	W	D	P	W	D	
<i>o</i> Cet	328.5/328.5	28/28	39/33	334.0/332.0	35/35	57/48	331.5	27	25	332.0
IK Tau ¹	475.5/471.0	94/100	29/15	453.2/452.0	100/99	-3/-20	467.5	129	2	470.0
TX Cam	540.0/542.0	66/69	82/67	532.3/533.0	98/106	64/77	542.5	79	44	557.4
R Cnc ^{3,4}	357.5/350.0	44/48	62/68	371.0/375.0	63/70	48/47	362.0	27	-6	361.6
R LMi ^{2,3}	375.0/376.5	36/36	42/47	375.0/378.0	34/38	46/59	374.5	27	-10	372.2
R Leo ²	311.5/312.5	24/25	32/29	304.5/304.0	23/23	16/28	314.0	21	10	310.0
W Hya ^{2,3,4}	390.0/391.5	111/61	5/26	394.5/393.0	61/64	10/33	384.5	29	-8	361.0
U Her ^{2,3,4}	403.0/403.5	58/58	77/58	417.0/428.0	64/122	71/74	403.5	38	25	406.1
R Aql ⁵	299.5/299.0	32/33	-5/3	299.0/296.0	40/45	-28/-10	279.5	17	0	284.2
R Aqr ⁴	394.0/393.5	36/39	59/57	400.0/395.0	47/42	45/38	397.0	36	9	387.0
“							395.5	42	38	387.0
R Cas ²	440.5/436.5	51/51	57/55	434.5/435.0	40/44	43/31	434.5	40	12	430.5
IRC+10011 ¹	579.5/587.5	236/238	27/10	635.5/642.0	138/139	-36/-44	650.5	234	-55	660.0
GY Aql	460.0/455.0	54/49	40/38	459.5/457.0	51/51	52/54	461.5	76	-10	204.0

P: Peak of temporal power spectrum (days). W: Half power width of main peak (days). D: Delay with respect to Optical Max. (days). In bold face only if the delay is with respect to the NIR.

¹ No optical data, curves and delays with respect to IR. ² Possible low frequency component.

³ Possible high frequency component. ⁴ Possible harmonics. ⁵ Power spectrum with low SNR.

The new information presented here (in terms of number of spectra) is 46% in $v = 1$ and 50% in $v = 2$ of the total data in the monitoring. They represent a fraction of around 80% if we consider only the data recorded after the major improvements on the receiver that were performed in December 1988. It is thus clear that the information presented in this final data set allows a re-examination of the different possible conclusions presented in ALC99 and MAR88. In particular, the large data set and its quality allows a time-series analysis in order to compare SiO variability with optical and near-IR curves, when available.

3. Time-series analysis of recorded SiO data

To investigate the temporal characteristics of the SiO light curves we need to use a maximum-likelihood estimator of the power spectrum of a curve, valid for unevenly sampled data, as is the case. We have chosen the Lomb-Scargle (LS) power estimator (Lomb 1976; Scargle 1982), which essentially consists of a least-squares fitting of the data to a sine function, whose period varies across the range of the power spectrum we want to sample. The results of the time-series analysis applied to our SiO data are summarized in Table 2. Since we are interested in comparing the SiO periods with those of the pulsation of the star, we have also applied the same method to the available light curves in the optical and/or in the NIR (LeB93). The results are also shown in Table 2. We must point out that for SiO we have applied the LS-power estimator to the logarithm of the SiO light curves instead of directly to the curves themselves. The reason for this is that for objects with a very high SiO contrast, (defined as the flux ratio between epochs of maximum and minimum emission), as in *o* Cet for instance (see Fig. 8), the LS-power estimator would have been too sensitive to flux differences at epochs of maxima, if applied directly to

the data. In addition, in this case the time-series analysis of the logarithmic SiO curves gives results with higher S/N ratio in the power spectrum. For stars with low SiO contrast, such as IK Tau, direct (i.e. non-logarithmic) analysis of the data is however probably the best choice, but the results from the logarithmic curve are still acceptable. To keep this analysis as simple and uniform as possible we have chosen to strictly follow the same method (i.e. to apply the LS algorithm to the logarithm of the SiO fluxes) for all stars. Note also that the optical and NIR curves are in fact on a logarithm scale, since they are given in magnitudes. In some cases where the time-series analysis does not give a power spectrum of high enough quality, one could easily figure out simple methods to better show up regularities in the variability of the SiO emission and improve the results, such as the subtraction of a linear baseline (see the case of VX Sgr in Sect. 4.2 and Fig. ??). However, to be rigorous, we have chosen not to apply any particular treatment in the algorithm in any case.

For objects showing regular SiO variability, established by a SiO period similar to the pulsation of the star found in our time series analysis, we have also computed the phase at which SiO maxima occur with respect to optical and/or NIR maxima. To do this we have computed the correlation between a cosine function having the same period and amplitude as the optical/NIR curves with the logarithmic SiO light curves. This correlation has been estimated for cosine functions with different phase delays with respect to the optical/NIR maxima. The delay between the SiO and the optical/NIR curves is then given by the delay of the cosine function that results in a maximum correlation value. We should first define for each individual star the corresponding cosine function with zero delay. This has been done by computing directly from the optical/NIR data the epochs of maxima in their curves, for the time-span of

the SiO monitoring only. We have not included possible maxima where either the previous rise or the following fall are not available in the data. The mean period and date for phase zero were then determined by a least-squares fitting of a straight line to the previously obtained dates vs. the number of periods since the first in the series: the slope of the line gives us the period in days, and the offset at period zero gives us the date for phase zero. The results of this correlation analysis for the stars with suitable data are shown in Table 2.

The reason we did not directly correlate the SiO data with the optical data is because this would have resulted in a wrong estimation of the phase of the SiO maxima with respect to the optical maxima. This is due to the nature of the optical light curves of Mira-type variables, which are not symmetric (see figures). The optical minima do not occur at phase 0.5 but rather typically at phase 0.6 to 0.7 depending on the asymmetry of the light curve. This implies different durations for the rising and falling sections of the curve, the latter being usually larger than the former. Because of this, a direct correlation between the optical data with a pure cosine function of identical period and null phase results in phases for the optical data itself of the order of 0.05–0.1, while they should obviously be zero. We have tested this effect numerically with the results also shown in Table 2. This spurious phase delay of the optical data is larger in TX Cam, most probably due to its particularly bad optical coverage compared with other objects, and in ρ Cet and U Her, precisely the Mira stars in our sample that show the most asymmetric optical light curves. Obviously, direct correlation of the optical and SiO data, would have resulted in phases for the SiO maxima which would have been wrong (smaller) by similar amounts.

4. Discussion

To avoid redundancy with some aspects already discussed in ALC99 we will focus our discussion on the characteristics and implications of the SiO maser emission shown by the different groups of objects under investigation. Only discussions on some individual objects, for which the new data provide interesting information not yet reported, will be given in the subsection about Regular Variables. For any other details about the individual objects, the reader is referred to ALC99.

4.1. Young stellar objects

Of the three SiO maser sources known among young stellar objects, Orion IRC2, Sgr B2(M) and W51-IRS2, the continuum of the latter has been monitored for the entire duration of the project to check calibration issues (see ALC99).

Recent VLBI images of the $v = 1$ $J = 2-1$, $v = 1$ $J = 1-0$, and $v = 2$ $J = 1-0$ SiO masers in the Orion-KL nebula (Doeleman et al. 2002) have traced the outlines of an outflow at distances of 18 to 67 AU from a central protostar. The maser emission displays an X-shaped morphology and so it contradicts models in which the masers form in a rotating protostellar disk. In our monitoring (see Fig. 1), the new data compared to those already published in ALC99 display no noticeable changes in line shape and variability behavior.

4.2. Supergiants

This group is represented in our sample by three objects: VY CMa, an M5-type star, μ Cep, of M2 spectral type, and VX Sgr, an M4-M10 object. The optical and SiO data are somewhat contradictory within this small sample (Figs. 2–4).

VY CMa and VX Sgr present clear optical cycles with amplitudes of about 1 and 3 mag and periods of 1528 and 791 days respectively. However, the SiO emission of these two objects is somehow erratic. It is worth pointing out, in addition, that the optical period of VY CMa does not agree with the 989 days found by Herman & Habing (1985) from 1612 MHz OH maser emission. In this same object, the tentative correlation pointed out in ALC99 between SiO and optical variations is not confirmed by the new data. There is in fact a minimum of SiO emission coincident with the optical maximum around MJD¹ 48 900. The main features of the SiO line profiles in VY CMa have been maintained during the 11 year period, especially the strongest spike centered at 22.5 ± 0.5 km s⁻¹. Only a small velocity drift of a few km s⁻¹ in the line centroid is noticeable due to the appearance of weak secondary peaks between ~ 33 and 39 km s⁻¹. In VX Sgr the situation is not much clearer: only if we look at the area of the $v = 1$ SiO transition does a coincidence of optical and SiO maxima seem to be present. Nevertheless the main feature in the SiO light curves is a secular weakening by about a factor of 5 in 3500 days. Greenhill et al. (1995) reported a ring-like distribution of the SiO maser emission with a radius of about $1.3 R_*$ from 1992 observations. However, by the end of this project VX Sgr was barely detectable in the two SiO maser lines. Therefore we cannot even say that SiO masers in supergiants are always as intense as they seemed by looking at the data presented in ALC99.

On the other hand, the predictions of a decrease in the SiO emission of μ Cep after MJD 48 031, made in ALC99, have been confirmed by the new data and it looks like we have just covered one SiO period (this period would be about 2900 days) while the optical emission has been fluctuating by 1.7 mag at most with no regular behavior. The SiO contrast is very large in both $v = 1$ and $v = 2$ SiO light curves since the masers are not detected after MJD ~ 49 200 and the maximum peak fluxes exceeded 500 Jy in both transitions around MJD 48 000.

From the above results, i.e. two objects with periodic optical variability and poor regularity in the SiO variability, and one object with possible well defined SiO periodicity and no well defined optical variability trends, we conclude that the variability of SiO masers in supergiants is much more complex than in Mira-type variables.

4.3. Semiregulars

Of the two stars initially classified in this group, the monitored SiO lines in GY Aql have shown a behavior similar to those in other Mira-type stars of our sample and are thus discussed in the following section. For the other one, RT Vir, it is not

¹ The dates in this paper will be given in Modified Julian Days (MJD = JD - 2 400 000.5).

really known if it is optically variable, but if it is, its amplitude is 1 mag at most. The SiO maser emission is weak and its variability erratic, with no signs of reproducibility. An OH maser monitoring of this object almost simultaneous with ours (Etoke et al. 2001) has shown a similar erratic behavior. In addition, 22 GHz H₂O maser monitoring of this object is available covering the period 1984–1998 (Lekht et al. 1999). The H₂O maser emission typically covers the same velocity range as that of 43 GHz SiO masers, $\sim 7\text{--}27\text{ km s}^{-1}$, and is well represented by a superposition of bursts from individual spectral features with no particular regularity.

4.4. Regular variables

We include in this group all Mira-type stars of our sample. GY Aql, classified as semiregular in ALC99, is also included in this group because our new SiO data reveal a very regular behavior. The OH/IR stars IRC+10011 and OH26.5+0.6 are also included in this group because their SiO emission shows periodicity, with somewhat longer periods than typical Miras, despite the unavailability of optical data. These two objects are probably Mira-type variables with a very thick molecular envelope that makes their detection at optical wavelengths very difficult. X Hya and χ Cyg are the only Mira-type stars in our sample for which no SiO period could be derived. Nevertheless, from the AAVSO data their optical periods have been established at 304 and 402 days respectively.

The main aim of this 43 GHz SiO monitoring is to study in detail the various aspects of the time variation of the two selected lines and its relationship with the variability of the hosting star at other wavelengths. To achieve this goal, the objects where an SiO period can be established are the best. The short time span of previous monitorings (see introduction) did not make it possible to perform numerical time-series analysis of the SiO data to quantitatively probe the result that, at least for Miras, the SiO intensity follows a regular variation with a period similar to the pulsation of the star. However, different studies carried out in different periods of time (spanning a total of 10 years, from 1978 to 1987) found for the stars in common that the SiO masers always attained their maxima near the epochs of optical maxima. That result was taken as proof that the periodicities of optical and SiO light curves were practically the same. In fact, a simple consideration reveals that they must be exactly the same, or a harmonic, since if the SiO period would have any small difference with respect to the optical one, then finding the SiO and optical emission showing their maxima with any given phase lag would be highly improbable.

Our monitoring is long enough (up to 11 years and 130 spectra in some cases) to allow a numerical study of the properties of the time fluctuations of the SiO maser emission at 7 mm. In addition, the number of objects suitable for the analysis is large. All Miras, together with GY Aql and the OH/IR stars, can be included, with the exception of X Hya and χ Cyg that have shown very weak SiO emission during the whole monitoring. In particular we can investigate for the first time the presence of other frequencies, besides the period of the star. The results of the analysis, following the methodology

described in Sect. 3, are given in Table 2. Figure 5 shows the power spectra of the time variability from the time-series analysis for 6 objects in our sample. The analysis has been done (when available) on the optical and NIR data in addition to the SiO data. For SiO, both peak and integrated area in $\nu = 1$ and $\nu = 2$ have been analyzed separately.

The presence of high frequency/low period components (i.e. harmonics of the main variability period) in some cases (R Cnc, W Hya, U Her and R Aql) is very probably due to the non pure sinusoidal variation of their SiO light curve. These components are also very prominent in some cases in the optical light curve, especially when the rising and falling parts of the curve do not have the same duration, see e.g. *o* Cet, R Aqr, R Leo and R Cas, in Figs. 8, ??, ??, and ??. In two cases, R Leo and R Cas, we have tentatively detected in SiO a possible low frequency component, with a period around twice the main one. This component could be due to the presence of alternating epochs of relatively strong and weak SiO maxima in R Cas, and to relatively irregular variation of the strength of the SiO maxima in R Leo. However, we must note that detecting variations with periods of about 2–3 yr or longer becomes very difficult, since considering the duration of the monitoring, it is expected that these long term components are affected by the limitations of the method.

Based on Table 2 we have built histograms showing the occurrence of SiO vs. optical and SiO vs. NIR phase lags in intervals of 0.05 periods. The counts in the histograms have been obtained as follows: for each object having regular variability, we consider the phase lag – with respect to the optical- of the peak and the area of both SiO lines explored (4 data points per object). For those objects where NIR LeB93 data are available, we consider the phase lags of the same 4 SiO curves with respect to the NIR. In the latter case we have a total of 12 data points, since only IK Tau, R Aqr and IRC+10011 are suitable objects. The resulting histograms are shown in Fig. 6. These histograms give first evidence of the following: a) the SiO maxima have a phase lag with respect to the optical maxima usually between 0.05 and 0.20 periods; and b) the SiO maxima appear to have almost no phase lag with respect to the NIR emission (at least in the 3–4 μm region).

The database presented here is admittedly still too limited to generally state that SiO maser emission reaches its maximum in phase with the NIR emission in long period Mira-type variables. The main problem is obviously the lack of NIR monitorings covering entire periods in a large enough sample of objects. Recently SMI03 have used the COBE DIRBE database to derive near- and mid-infrared light curves for a sample of 38 Mira-type variables. In their sample, 11 of our objects are present (*o* Cet, R Aql, R Cas, R Cnc, R Leo, R LM_i, TX Cam, U Her, IK Tau, IRC+10011 and R Aqr, the last three also in LeB93). Although the data are fragmentary between MJD $\sim 47\,850$ and $48\,150$ (see Fig. 7) and in none of the objects cover one entire period, in three cases (R Cas, *o* Cet and R Aqr) they clearly support the conclusion indicated by the histograms. For the discussions in this paper we use only the 3.5 and 4.9 μm bandpasses of DIRBE, because they are very close in wavelength to those used in LeB93.

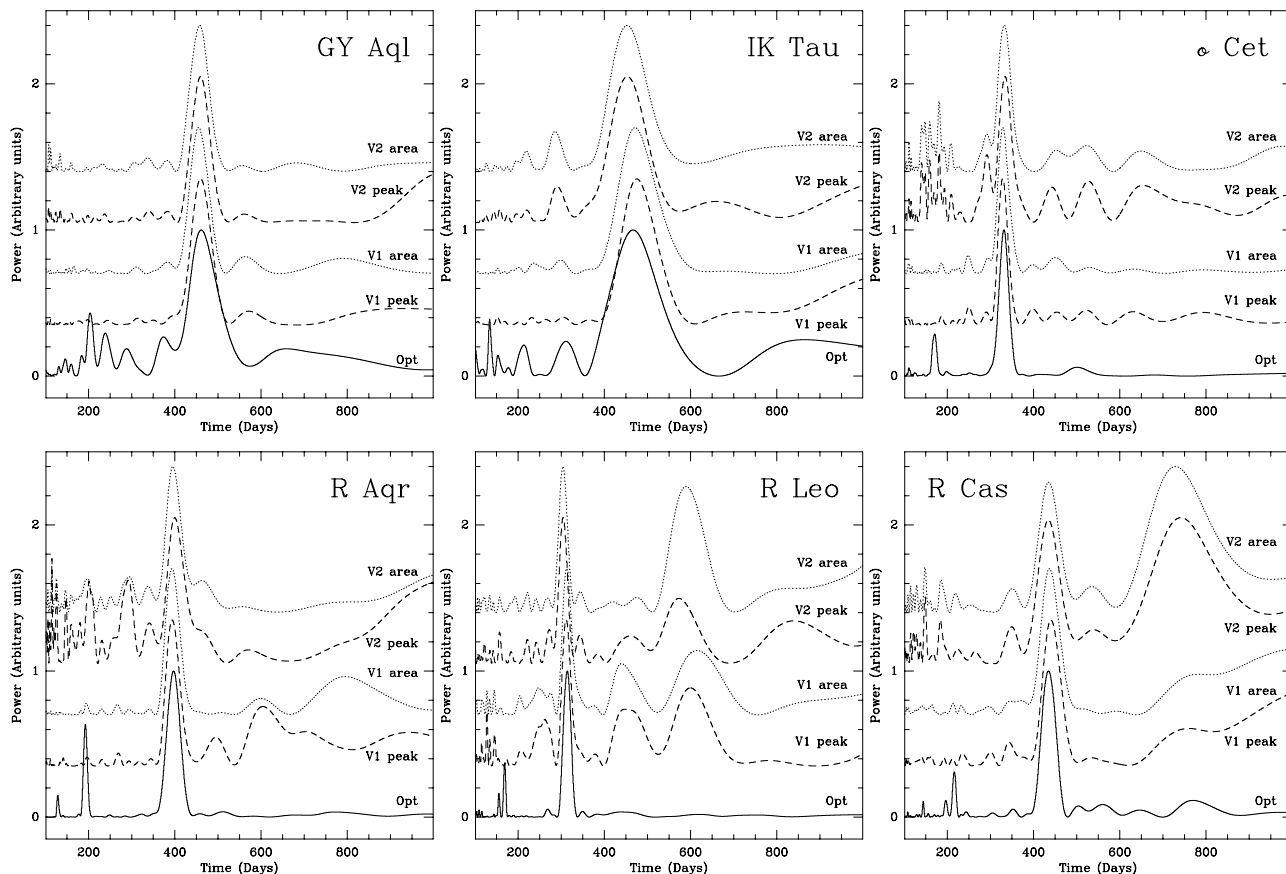


Fig. 5. Results of the time series analysis for 6 regular variables in our sample. This figure provides information only on the variability periods in optical and SiO (both peak and integrated area in $v = 1$ and $v = 2$). The complete information obtained from this analysis for all suitable objects, including delays between SiO and optical or NIR maxima is provided in Table 2.

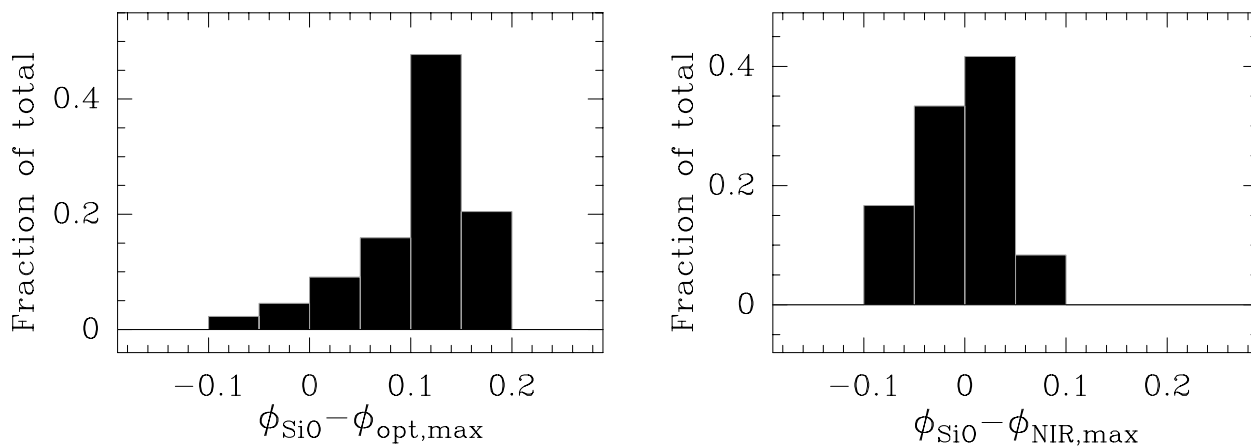


Fig. 6. SiO versus NIR and Optical phase lag histograms for a sample that consists on the four SiO delays listed in Cols. 4 and 7 of Table 2 for those objects where suitable optical (from the AAVSO) and/or NIR (from LeB93) data exist.

The best example is R Cas. Although there is a gap in the DIRBE coverage at the moment of the NIR maximum, this occurred presumably between MJD 47970 and 47990, i.e. 54 to 74 days after the optical maximum (JD 2447916). From the overall SiO data, our time series analysis (Table 2) gives an optical-SiOV1 delay of 56 days whereas the optical-SiOV2 delay is established at 35 days.

A second good example is *o* Cet. The NIR data start on JD 2447873, the flux is almost constant for about 20 days, possibly indicating a maximum, and then it decreases. If the interpretation of the NIR data is correct, this maximum coincides exactly with a well detected SiO maximum happening between MJDs 47861 and 47900, and both are delayed some 40 to 70 days with respect to the optical maximum (MJD 47819).

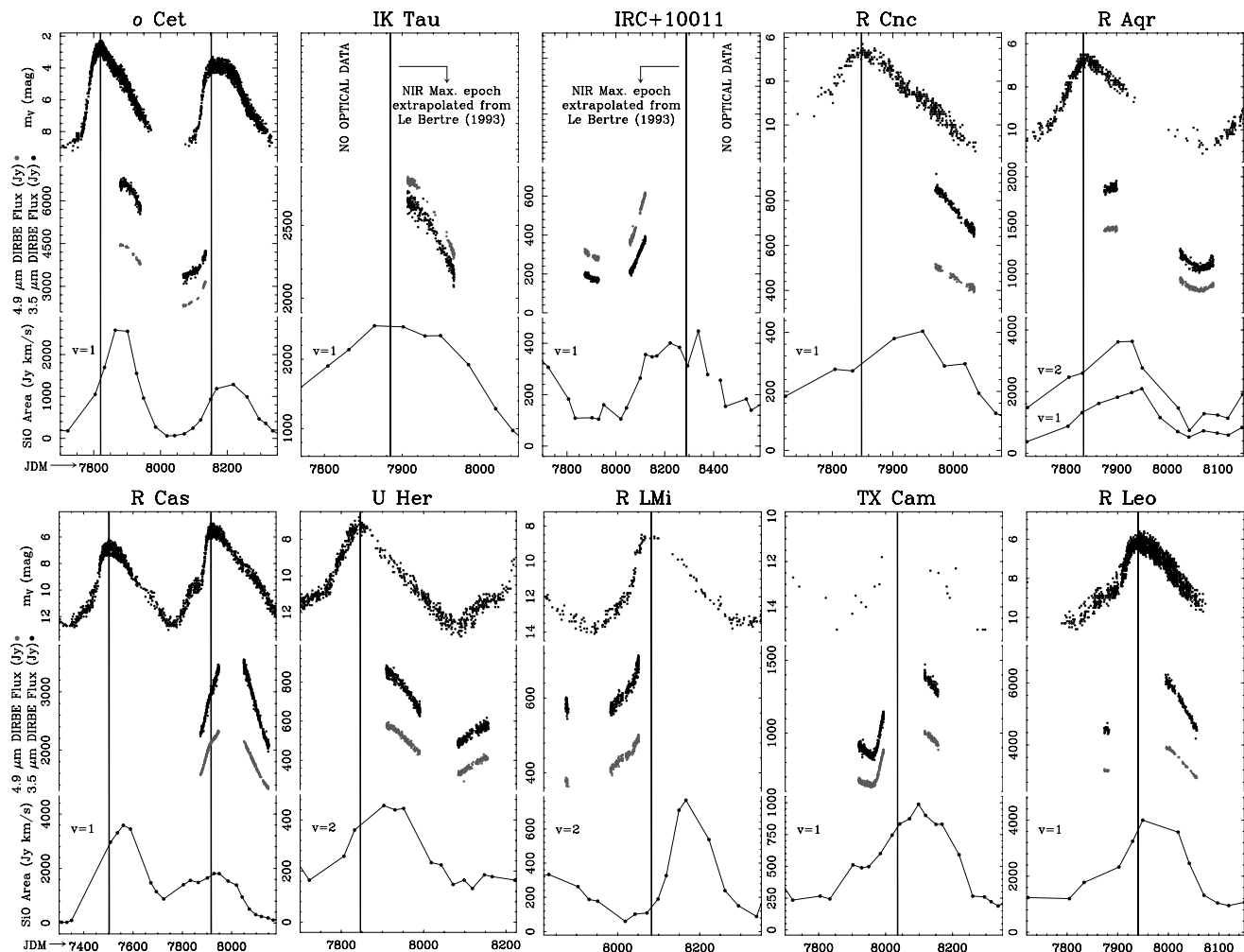


Fig. 7. Comparison of optical, SiO, and NIR (Smith et al. 2002, 2003) light curves in a subset of objects from our sample. The cases of *o* Cet, R Aqr and R Cas are of particular interest (see text). Dates of optical maxima are indicated by vertical lines unless otherwise indicated.

The average optical-SiO delay from our time series analysis of this object is 44 days. The NIR data corresponding to U Her might possibly also have led to a similar conclusion should the DIRBE coverage have started only a few days earlier.

The third good example is R Aqr. This object is the only one for which optical, SiO, and NIR (both LeB93 and SMI03) data are available. SMI03 data report a minimum at MJD 48 065 (with practically no lag with respect to the corresponding optical and SiO minima) and possibly a maximum at MJD 47 890 or later. This maximum is delayed about 55 days or more with respect to a sharp optical maximum (MJD 47 835). The average optical-SiO delay from the time series analysis is 50 days for this object.

In the other objects the SMI03 NIR data do not provide enough information around epochs of SiO maxima to extract similar conclusions. However in all cases we see that NIR decreases or increases match the same behavior in the SiO and optical light curves.

Some objects in this group require additional separate comments.

4.4.1. *o* Cet

The trend shown by the data presented in ALC99, i.e., rapidly decreasing intensity of consecutive maxima, continued after MJD 48 000 for at least 4 periods during which the SiO emission was almost undetectable even at the expected maxima. A good recovery occurred in the maximum expected around MJD 49 480, with peak fluxes greater than 1000 Jy. This object is thus the best example of the poor reproducibility of the SiO variability amplitude from one period to another. A second modulation with a much longer period could be present and its explanation could be related to the fact that the red giant responsible for the SiO emission belongs to a multiple system. See recent results on the role of the companion(s) in shaping the morphology of the SiO emitter circumstellar environment in Karovska et al. (1997) and Marengo et al. (2001).

All the new SiO data presented in this paper confirm very nicely the phase lag between optical and SiO emission (our time series analysis has established it at 0.13 for this object). The comparison with the NIR data from SMI03 (Fig. 5) suggests that an SiO maximum and an NIR maximum occurred

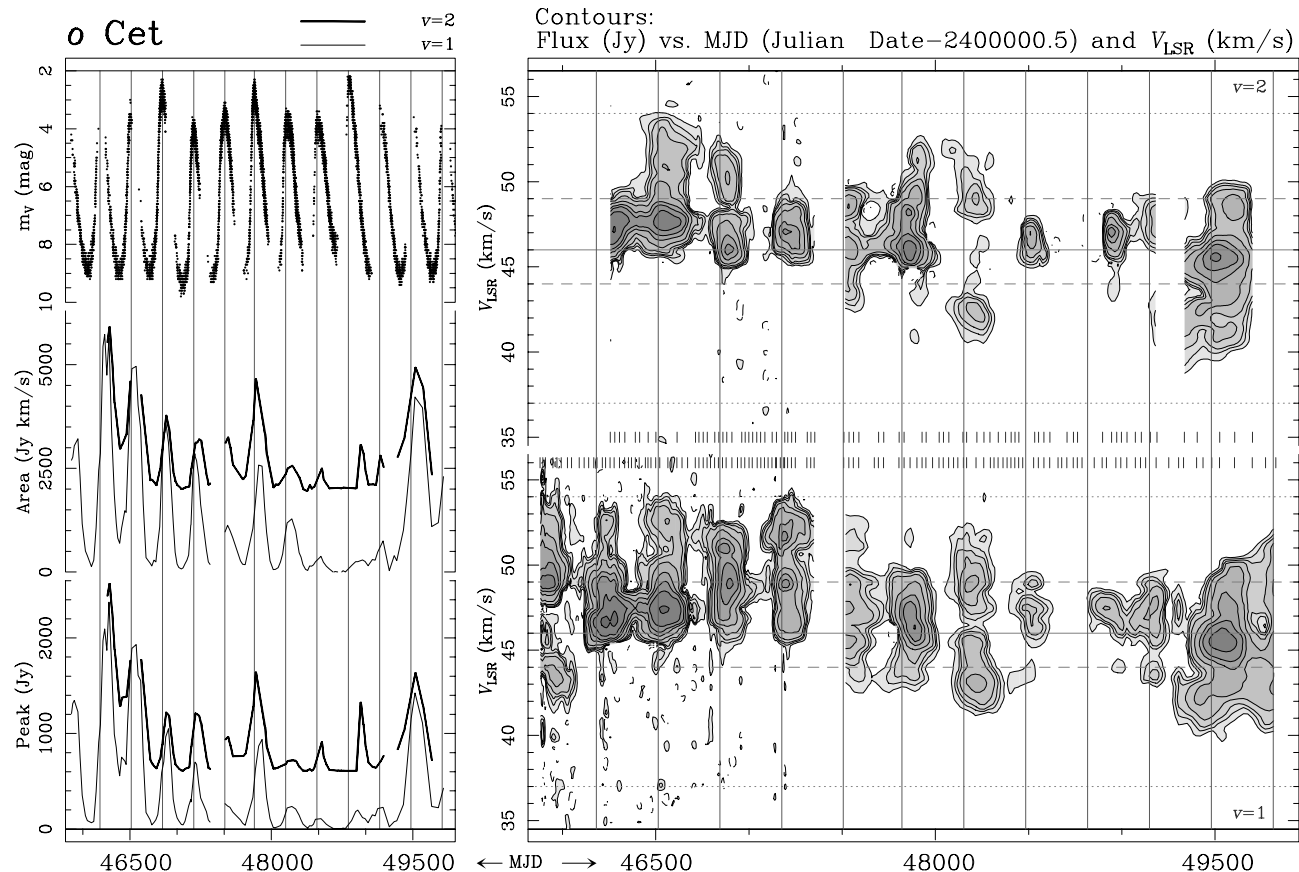


Fig. 8. *Left:* optical and $^{28}\text{SiO } v = 1, 2 J = 1-0$ light curves of *o* Cet (Mira) between mid 1984 and mid 1995. The $v = 2$ curves have been shifted by 600 Jy (peak) and 2000 Jy km s $^{-1}$ (area) for clarity. *Right:* time evolution of the monitored SiO lines as a function of LSR velocity. The contours mark the following flux levels (in Jy): 20, 40, 60, 100, 200, 400, 600, 1000, and 2000 for both $v = 1$ and $v = 2$. Dates of optical maxima are indicated by vertical lines. The solid horizontal line in the right panels represents the velocity of the CO $J = 2-1$ peak emission, the dashed horizontal lines are the velocities at which the CO emission is half of the peak, and the dotted horizontal lines represent the terminal velocities at which CO emission disappears (from Cernicharo et al. 1997). The small vertical ticks mark the dates of observations.

simultaneously around MJD 47 875, more than 50 days later than the corresponding optical maximum.

4.4.2. GY Aql

This star was classified as semiregular in our sample at the beginning of the project, yet its SiO maser emission has been revealed as extremely regular in the last part of the survey (Fig. 9). Optical observations in the last few years, reported here for the period of time coincident with our monitoring, now provide an optical period of 461.5 ± 76 days (see Table 2), remarkably similar to the SiO period. The high SiO contrast, larger than 4, and the integrated flux ratio between $v = 2$ and $v = 1 \sim 1$ are both similar to what is typically found in Mira-type variables.

4.4.3. IK Tau

The VLBI images by Boboltz & Diamond (2000) show that the SiO masers are distributed in an axisymmetric ring roughly 29×16 milli-arcsec with position angle of ~ 59 deg. The semimajor axis of the elliptical distribution also provides an axis of symmetry for the velocity structure of SiO masers,

with blue-shifted features ($29-35$ km s $^{-1}$) lying to the northwest and red-shifted features ($35-41$ km s $^{-1}$) lying to the southeast. Similar velocity components appear in our data from MJD 46 000 to MJD 48 400 approximately (Fig. 10). The most remarkable feature of our SiO data in this source is the persistence of velocity components over several periods, probably indicating a survival of the basic masing clumps for several pulsations. Afterward, the two mentioned velocity components merged into only one extending $\sim 32-38$ km s $^{-1}$.

The large excess of IR emission in this object was monitored by LeB93 for nearly 3 stellar periods at 3.79 and $4.64 \mu\text{m}$. These data make it possible to calculate a NIR period and to extrapolate to the future the epochs of NIR maxima yielding a remarkable coincidence with SiO maxima. The numerical evidence is provided in Table 2 where, of the four SiO curves analyzed (peak and integrated flux emission in $v = 1$ and $v = 2$), the lag of the SiO maxima with respect to the NIR never exceeds 0.06 periods.

4.4.4. R Aqr

This symbiotic stellar system, consisting of a Mira-type variable and a hot dwarf companion surrounded by an accretion

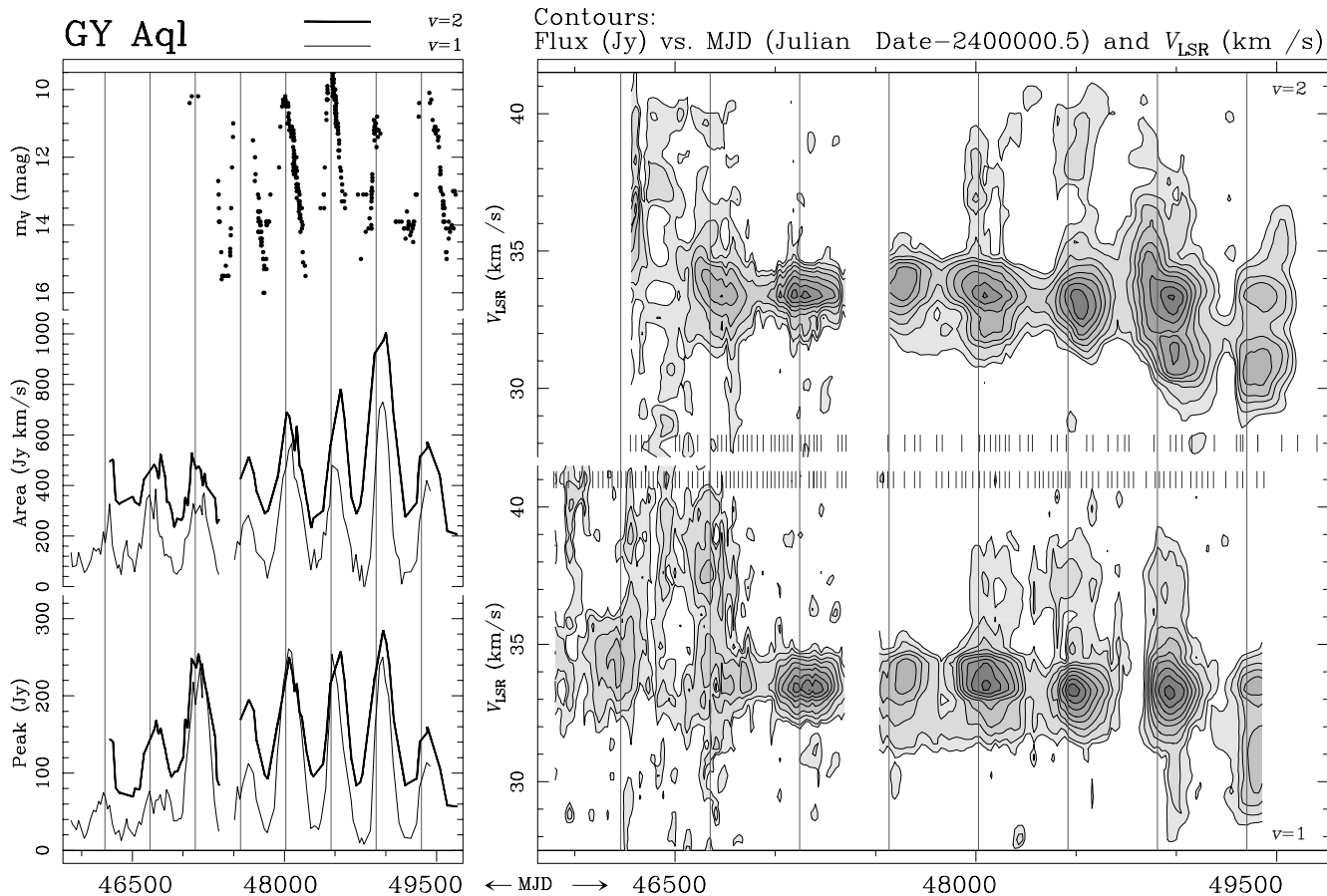


Fig. 9. Same as Fig. 8 but for GY Aql. The CO velocities are not shown in this case. The $v = 2$ curves on the left panel have been shifted by 50 Jy (peak) and 200 Jy km s⁻¹ (area) for clarity. The contour levels for SiO are: 10, 20, 40, 60, 90, 120, 160, 200, and 250 Jy for both $v = 1$ and $v = 2$.

disk orbiting with large eccentricity (~ 0.8) and a period of ~ 44 yr, is one of the few examples of such systems where SiO maser emission has been detected. The new data presented in this paper (after MJD 48 031) correspond in general to much stronger emission than previously reported. The behavior is similar to that of any other strong Mira-type SiO emitter. In fact, Hollis et al. (1997) have reported that the system might have been at apastron in 1996, and therefore the Mira-type variable would have been little influenced by the hot companion/accretion disk in the last part of our monitoring. This was confirmed by the VLBI observations presented by Boboltz et al. (1997) where the $v = 1$, $J = 1-0$ SiO maser was reported to form ringlike structures typical of isolated Mira variables. The four new maxima presented in this paper are clearly shifted with respect to the optical maxima in approximately the same way as the NIR data reported by LeB93. SMI03 report a minimum at MJD 48 065 and possibly a maximum at MJD 47 880, both coinciding with a well defined SiO minimum and maximum, the latter occurring some 50–60 days later than one of the optical maxima. If the orbital data are correct, it is expected that the SiO behavior of this object will be noticeably different from the one of isolated Mira variables reported here at some moment around the years 2015 to 2021, when the hot companion would be from 5 to 9 times closer to the Mira-type star than it was at the end of our monitoring.

4.4.5. IRC+10011

The 3 NIR maxima beyond MJD 48 000 predicted from the LeB93 data are in very good agreement with the observed $v = 1$ and $v = 2$ SiO maxima. The NIR data reported by SMI03 indicate a minimum at MJD 47 900–47 930, in perfect agreement with one of the SiO minima. Unfortunately, their NIR data for this object stop at MJD $\sim 48 140$, with the flux quickly increasing, and the predicted maximum based on LeB93 occurs at MJD 48 287.

4.4.6. OH 26.5+0.6

The SiO maximum at MJD $\sim 47 950$ reported by ALC99 was followed by another much stronger maximum at MJD $\sim 49 580$. Although we have recorded only these two SiO maxima in this survey, they suggest a SiO period of about 1640 days, very close to the period of 1600 days found by Herman & Habing (1985) from 1612 MHz OH maser emission measurements.

4.4.7. R Leo

The SiO variability of this star has become clearer with the new data presented here with respect to ALC99. The time series analysis provides an SiO period coincident to within 10 days

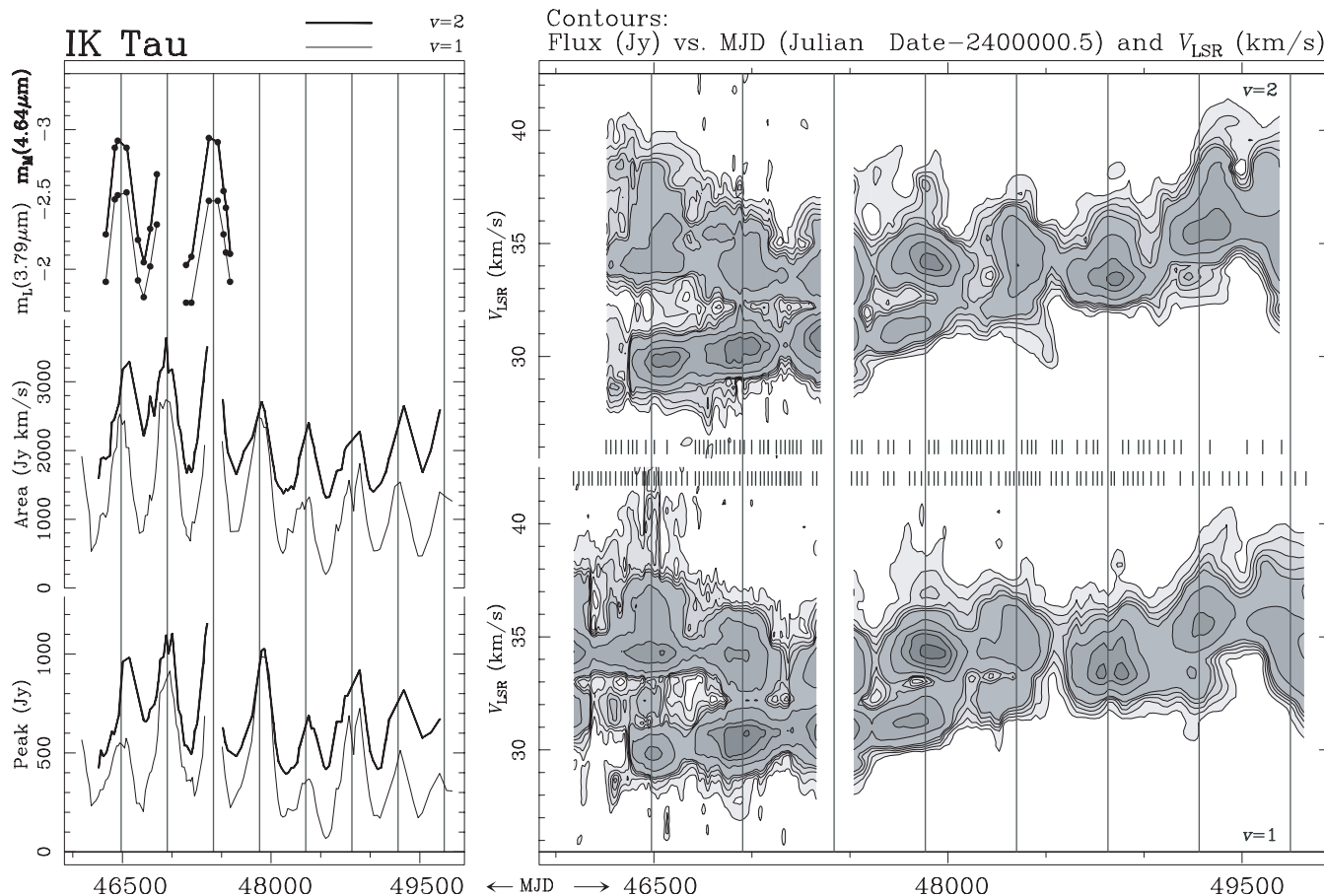


Fig. 10. *Left:* near-Infrared ($3.79 \mu\text{m}$, dots connected by a black solid line, and $4.64 \mu\text{m}$, dots connected by a blue solid line) and $^{28}\text{SiO } v = 1, 2 J = 1-0$ light curves of IK Tau. The $v = 2$ curves on the left panel have been shifted by 300 Jy (peak) and $1000 \text{ Jy km s}^{-1}$ (area) for clarity. From the time series analysis of optical, NIR and SiO light curves the periods have been determined (see Table 2) and they all are in remarkable agreement. This object, together with R Aqr, is a good example for showing that NIR and ^{28}SiO light curves have very little phase lag. The right panels show the time evolution of the monitored SiO lines as a function of LSR velocity. The contours mark the following levels (in Jy): 20, 40, 60, 80, 100, 200, 400, 600, and 900 for both $v = 1$ and $v = 2$ in IK Tau.

with the optical one (see Table 2). In this star the SiO emission at minimum remains relatively strong, above 800 Jy km s^{-1} in most cases, and the changes in the line profile are quite large. A maximum of this star was monitored with a time resolution of one day in Aug.–Sep. 1992 (Pijpers et al. 1994). The date of the SiO maximum could be precisely determined: MJD 48 879, 21 days (phase 0.07) after the AAVSO optical maximum.

5. Conclusions

The complete results have been presented of the longest short-spaced monitoring of SiO maser emission in evolved stars carried out to date. Of a total of 21 objects in the sample, we have covered more than 8 full cycles for 13 regular variables, mostly Mira-type stars. This has provided a unique database to calculate periods and to derive the main features of SiO variability in this type of stars. The key for the success of the project has been the careful observing procedure aimed at ensuring a good relative calibration of the spectra over the years. In fact, the time-span of the database is long enough to perform a time series analysis from which the SiO periods have been

quantitatively determined. The results show that all SiO periods are within $\pm 4\%$ of the optical period given by the General Catalog of Variable Stars or those directly calculated from the time series analysis of the optical light curves. From the same analysis, it has been shown that the SiO maxima occur with a phase lag mostly between 0.05 and 0.20 periods with respect to the optical maxima. A histogram (Fig. 6) clearly shows the trend. Comparison with available, although fragmentary, NIR light curves has given clear evidence in several objects that the SiO and NIR maxima occur practically in phase. Therefore, the data shown in this paper make it possible to address, with the best observational support to date, the question of what type of pumping (collisional or radiative) is responsible for the observed SiO masers in the types of objects under consideration.

A natural consequence of radiative pumping models is that SiO maser light curves have the same period as the star at optical or IR wavelengths, and that they are in phase with the NIR variability (see Bujarrabal 1994a,b). The reported variations in the maximum/minimum contrast of the SiO cycles would suggest that other phenomena such as variations in the amount of mass in the emitting region in each pulsation also

play a role. Additional arguments favoring radiative pumping can be found in Desmurs et al. (2000), Bujarrabal et al. (1987, 1994a,b, and references therein).

On the other hand, collisional pumping models explain the coincidence of the SiO and optical periods assuming that a shock wave originates at the stellar surface and reaches, typically after about some hundreds of days, the masing region, changing its SiO emission properties (Humphreys et al. 2002). The main concern we have about such an scenario is the difficulty of explaining the phase coincidence of the SiO and NIR variabilities revealed by our data (see Fig. 6). The phase lag of the shock arrival with respect to the optical maxima depends on a number of parameters, such as the sizes of the star and of the SiO emitting region, the shock velocity, and the period, that are known to vary significantly for the objects in our sample. Therefore, two coincidences are necessary for the collisional pumping models to explain the observations: the shock arrival phase must be the same for all stars, and the phase at which the wave initially leaves the photosphere must be such that the arrival phase in the SiO maser ring (itself changing diameter during a stellar pulsation) is equal to the NIR maximum phase. In fact, Cotton et al. (2004) found, from their VLBI data on several stars, that the phase between SiO maser ring diameter and luminosity was not consistent among different stars.

Our work indicates a tight and universal SiO/NIR phase coincidence, making a strong case in favor of radiative pumping of SiO masers, which explains such a correlation in a very natural way.

Acknowledgements. The observational and technical work involved in the Yebes SiO maser monitoring amounts to several thousands of hours in 11 years. We acknowledge the collaboration of all the astronomers and technical staff of the Observatory. Several databases have been used in this research that are gratefully acknowledged: the AAVSO International Database, based on observations submitted to the AAVSO by variable star observers worldwide, the NIR observations of IRC+10011, R Aqr, IK Tau and VY CMa provided by T. Le Bertre, and the COBE-DIRBE NIR light curves of 11 objects kindly provided by B. Smith. We thank support for this work from Spanish DGES grant AYA 2000-0927. J. R. Pardo's research is currently supported by Spanish PNIE and DGES and grants ESP2002-01627, AYA2002-10113-E and AYA2003-02785-E. The operations of the Observatorio Astronómico Nacional 13.7 meter telescope at the Centro Astronómico de Yebes have been financially supported by several Spanish DGES projects, the last one involving the SiO monitoring under code PB96-0104.

References

- Alcolea, J., Pardo, J. R., Bujarrabal, V., et al. 1999, A&AS, 139, 461 (ALC99)
- Barcia, A., Bujarrabal, V., Gómez-González, J., Martín-Pintado, J., & Planesas, P. 1985, A&A, 142, L9
- Barvainis, R. E., McIntosh, G., & Predmore, C. R. 1987, Nature, 329, 613
- Boboltz, D. A., Diamond, P. J., & Kemball, A. J. 1997, ApJ, 487, L147
- Boboltz, D. A., & Diamond, P. J. 2000, Am. Astron. Soc. Meet., 197, #45.07
- Bujarrabal, V. 1994a, A&A, 285, 953
- Bujarrabal, V. 1994b, A&A, 285, 971
- Bujarrabal, V., Planesas, P., & del Romero, A. 1987, A&A, 175, 164
- Cernicharo, J., Alcolea, J., Baudry, A., & Gonzalez-Alfonso, E. 1997, A&A, 319, 607
- Cotton, W. D., Mennesson, B., Diamond, P. J., et al. 2004, A&A, 414, 275
- Desmurs, J. F., Bujarrabal, V., Colomer, F., & Alcolea, J. 2000, A&A, 360, 189
- Doeleman, S., Lonsdale, C., Kondratko, P., Raas, W., & Predmore, C. R. 2002, Cosmic masers: From proto-stars to black holes, IAU Symp., #206, held 5–10 March 2001 in Angra dos Reis, Rio de Janeiro, Brazil, ed. V. Mineese, & M. Reid (San Francisco: ASP), 290
- Etoka, S., Blaszkiewicz, L., Szymczak, M., & Le Squeren, A. M. 2001, A&A, 378, 522
- Glenn, J., Jewell, P. R., Foure, R., & Miaja, L. 2003, ApJ, 588, 478
- Greenhill, L. J., Colomer, F., Moran, J. M., et al. 1995, ApJ, 449, 365
- Diamond, P. J., & Kemball, A. J. 2003, ApJ, 599, 1372
- Herman, J., & Habing, H. J. 1985, A&AS, 59, 523
- Herpin, F., Baudry, A., Alcolea, J., & Cernicharo, J. 1998, A&A, 334, 1037
- Hjalmarson, Å., & Olofsson, H. 1979, ApJ, 234, L199
- Hollis, J. M., Pedelty, J. A., & Lyon, R. G. 1997, ApJ, 482, L85
- Humphreys, E. M. L., Gray, M. D., Yates, J. A., et al. 2002, A&A, 386, 256
- Karovska, M., Hack, W., Raymond, J., & Guinan, E. 1997, ApJ, 482, L175
- Lane, A. P. 1982, Ph.D. Thesis, University of Massachusetts
- Le Bertre, T. 1993, A&AS, 97, 729 (LEB93)
- Lekht, E. E., Mendoza-Torres, J. E., Pashchenko, M. I., & Berulis, I. I. 1999, A&A, 343, 241
- Lomb, N. R. 1976, Ap&SS, 39, 447
- van Loon, J. C., Zijlstra, A. A., Bujarrabal, V., & Nyman, L. A. 1996, A&A, 306, L29
- Marengo, M., Karovska, M., Fazio, G. G., et al. 2001, ApJ, 556, L47
- Martínez, A., Bujarrabal, V., & Alcolea, J. 1988, A&AS, 74, 273 (MAR88)
- Nyman, L. A., & Olofsson, H. 1986, A&A, 158, 67
- Phillips, R. B., Straughn, A. H., Doeleman, S. S., & C. J., Lonsdale 2003, ApJ, 588, L105
- Pijpers, F. P., Pardo, J. R., & Bujarrabal, V. 1994, A&A, 286, 501
- Rausch, R., Kegel, W. H., Tsuji, T., & Piehler, G. 1996, A&A, 315, 533
- Scargle, J. D. 1982, ApJ, 263, 835
- Smith, B. J., Leisawitz, D., Castelaz, M. W., & Luttermoser, D. 2002, AJ, 123, 948
- Smith, B. J. 2003, AJ, 126, 935 (SMI03)
- Snyder, L. E., & Buhl, D. 1974, ApJ, 189, L31